JOURNAL OF SOLID STATE CHEMISTRY 111, 229–237 (1994)

The Solid Solution $BaFe_{12-2x}Co_xTi_xO_{19}$ ($0 \leq x \leq 6$): Cationic Distribution by Neutron Diffraction

M. V. Cabañas,* J. M. González-Calbet,†,‡ J. Rodríguez-Carvajal,§ and M. Vallet-Regí*,‡,[1]

*Dpto. Química Inorgánica y Bioinorgánica, Facultad de Farmacia, Universidad Complutense, 28040 Madrid, Spain; †Dpto. Química Inorgánica, Facultad de Químicas, Universidad Complutense, 28040 Madrid Spain; ‡Instituto de Magnetismo Aplicado, Apdo. 155, Las Rozas, 28030 Madrid, Spain; and §Lab. Léon Brillouin (CEA-CNRS), Centre d'Etudes de Saclay, 91191 Gif sur Yvette Cedex, France

Received May 20, 1993; accepted September 21, 1993

The solid solution $BaFe_{12-2x}Co_xTi_xO_{19}$ has been prepared in the range $0 \leq x \leq 6$. The crystal structure and cationic distribution between the different metallic sublattices of the magnetoplumbite structure have been refined from high resolution neutron powder diffraction data. Our results show that the preference of Fe^{3+}, Co^{2+}, and Ti^{4+} for the different sublattices can be modeled considering three regions in the whole compositional range. In this system, Co^{2+} has a preference for tetrahedral positions, probably due to the fact that Ti^{4+} has a stronger preference for octahedral positions. This fact explains why the end member of the series, $BaCo_6Ti_6O_{19}$, can be easily prepared. The hypotheses for the cationic distribution are validated by the reasonable agreement obtained from comparison of the average observed metal–oxygen distances with the expected distances from the valence bond approach for each site.

INTRODUCTION

M-type barium hexagonal ferrite ($BaFe_{12}O_{19}$) has generated great research effort in past years because of its relevance in technological applications such as permanent magnets, microwave devices, and recording media (1, 2). The substitution of certain ions in place of some Fe^{3+} ions in this highly anisotropic ferrimagnetic material produces substantial and interesting changes in its magnetic properties. In this sense, Co–Ti substituted barium ferrite particles are of great interest for high density magnetic recording applications (1–3).

The crystal structure of $BaFe_{12}O_{19}$ (space group $P6_3/mmc$, $Z = 2$) can be symbolically described with the ... RSR^*S^* ... sequence, where R is a three-layer block (O_4–BaO_3–O_4) and S is a two-oxygen-layer block (O_4–O_4); the * symbol indicates that the corresponding block has been turned 180° around the hexagonal c-axis (1, 4, 5). In this structure, five nonequivalent sublattices are present: three octahedral (in Wyckoff notation 2*a*, 12*k*, and 4*f*VI), one tetrahedral, 4*f*IV, and the remaining one indicated by 4*e*(1/2). The description of the atom occupying the bypyramidal cavity, centered in the Wyckoff position 2*b* (4), as pseudotetrahedral (4*e* site) with half occupation is just an artifice to mimic the strongly anharmonic motion presented by the Fe^{3+} ions in $AFe_{12}O_{19}$ (A = Ba, Sr) (5). The motion of the atom in the bypyramidal cavity can be considered to be a fast hopping between the two adjacent tetrahedra. The particular nature of this cavity is that the rest of the structure imposes an elongated trigonal bypyramid with a too-small central hole and too-far-away apical oxygens for the central 3*d* ions. The *M*-tape crystal structure is represented in Fig. 1.

From a magnetic point of view, $BaFe_{12}O_{19}$ is ferrimagnetic below $T_c \sim 723$ K and the magnetic structure is uniaxial collinear to the c-axis of the crystallographic structure (6, 7). The cationic substitution alters the critical equilibrium of the superexchange paths and leads to the appearance of new noncollinear magnetic structures (8, 9).

On the other hand, it is known that in the $BaFe_{12-2x}Co_xTi_xO_{19}$ system, the *M*-type structure remains along the $0 \leq x \leq 1$ range, in which the overall magnetic structure remains ferrimagnetic (9, 10) and the coercive field diminishes to technologically suitable values for magnetic perpendicular recording (3). This system has been studied using different techniques, but the results concerning the distribution of Co^{2+} and Ti^{4+} ions in Fe^{3+} sublattices are rather different (10–13).

We report in this work the synthesis, structural properties, and cationic distribution of the $BaFe_{12-2x}Co_xTi_xO_{19}$ solid solution in the $0 \leq x \leq 6$ range.

EXPERIMENTAL

Polycrystalline samples with composition $BaFe_{12-x}Co_xTi_xO_{19}$ ($0 \leq x \leq 6$) were prepared by high temperature solid state reaction from stoichiometric amounts of $BaCO_3$, α-

[1] To whom correspondence should be addressed.

0022-4596/94 $6.00

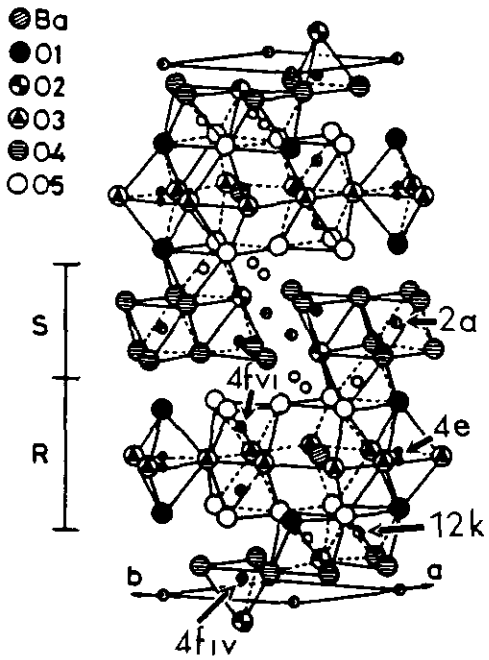

FIG. 1. Crystallographic structure and coordination polyhedra of $BaFe_{12}O_{10}$.

Fe_2O_3, TiO_2 (anatase), and Co_3O_4 raw materials. Different firing temperatures between 1000 and 1300°C were used during several days with intermediate grinding, in order to obtain a single phase. A black homogeneous powder was obtained after quenching in air.

X-ray diffraction was performed on a Siemens D-500 diffractometer (Cu$K\alpha$ radiation) and an X-ray Guinier camera (Fe$K\alpha$ radiation).

Neutron powder diffraction patterns were collected with the D1B and D2B diffractometers at the Institut Laue-Langevin (Grenoble, France). The wavelengths of the incident neutron beam were 2.519 and 1.594 Å, respectively.

RESULTS

A. X-Ray Powder Diffraction

X-ray powder diffraction data indicate that total substitution of Fe(III) by Co(II)–Ti(IV) ions is achieved. All samples show very similar diffraction patterns, all reflections being indexed on the basis of the magnetoplumbite-type structure, keeping the $P6_3/mmc$ space group. Table 1 shows the progressive increase of lattice parameters and cell volumes with increasing Co(II)–Ti(IV) content. A linear dependence according to Vegard's law (14) is observed for the cell volume (Fig. 2).

X-ray diffraction cannot provide information about the cation distribution due to the similar scattering power of all the ions involved.

TABLE 1

Unit Cell Parameters of the System $BaFe_{12-2x}Co_xTi_xO_{19}$ ($0 \le x \le 6$), Obtained from X-Ray Powder Diffraction Patterns

x	a (Å)	c (Å)	V (Å)
0	5.8929(5)	23.204(2)	697.8(1)
1	5.8940(3)	23.235(2)	699.08(3)
2	5.8957(4)	23.282(4)	700.8(1)
3	5.9000(3)	23.326(3)	703.19(6)
4	5.9062(3)	23.342(3)	704.99(6)
5	5.9132(6)	23.358(4)	707.2(2)
6	5.9174(8)	23.368(6)	708.6(2)

B. Neutron Powder Diffraction—Data Analysis

As the barium hexaferrite structure is retained over the composition range ($0 \le x \le 6$), the cationic distribution was studied by neutron diffraction, since the neutron scattering lengths of the doping atoms are quite different from that of Fe ($b_{Fe} = 0.954$, $b_{Co} = 0.25$, $b_{Ti} = -0.33$, all in 10^{-12} cm).

In order to obtain the cationic distribution, only the diffractograms corresponding to the paramagnetic phase were studied. The data were analyzed with the Rietveld method of the STRAP software package (15). The cell and positional parameters, together with the average scattering lengths, $\langle b^i \rangle$, corresponding to the five metallic sublattices of the magnetoplumbite-type structure, were simultaneously refined assuming the $P6_3/mmc$ space group. A strong correlation between isotropic temperature factors and average scattering lengths was observed. Then, a common isotropic temperature factor was assumed for the five metal sublattices. Another common temperature factor was assigned to the oxygen sublattices.

Figure 3 shows both the experimental and refined neutron diffraction patterns for $x = 4$ and $x = 6$.

As the scattering lengths of doping cations are smaller

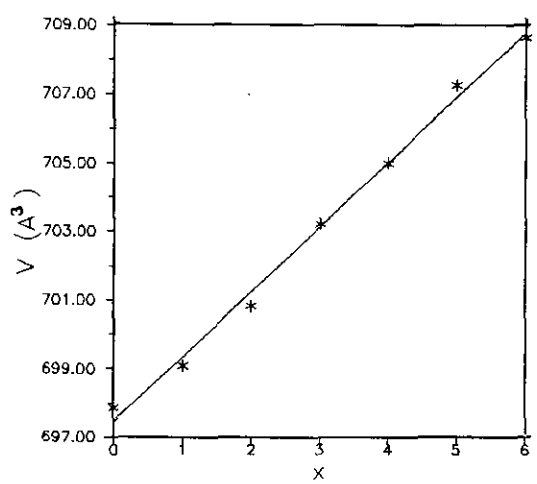

FIG. 2. Variation of the unit cell volume with composition.

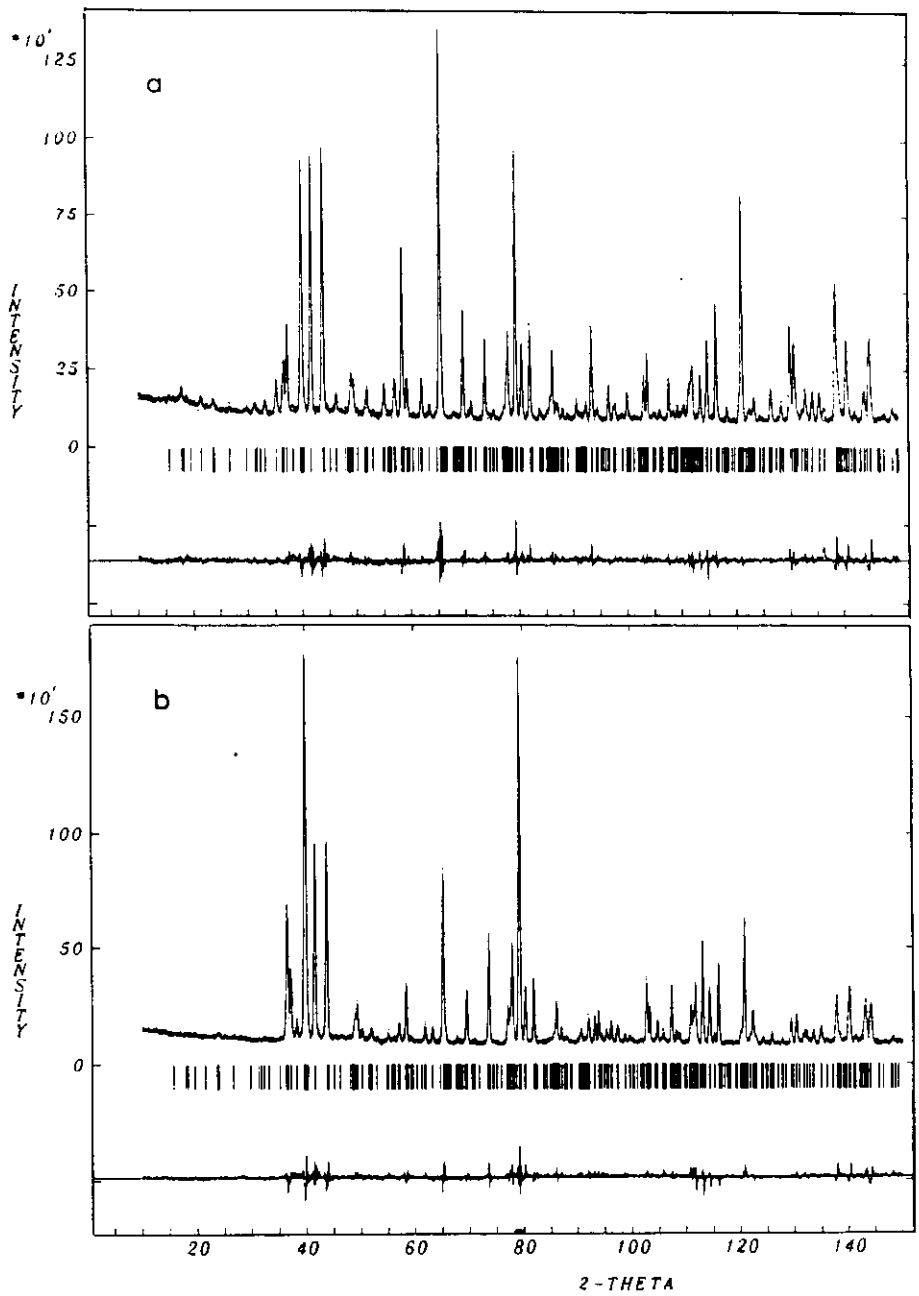

FIG. 3. Observed and calculated neutron diffraction patterns of (a) $BaFe_4Co_4Ti_4O_{19}$ and (b) $BaCo_6Ti_6O_{19}$ collected on D2B at 298 K.

than that of Fe, the average scattering length of each metallic sublattice ($\langle b^i \rangle$) must decrease when Co and Ti ions are introduced. For each sublattice where substitution takes place, we can write

$$\langle b^i \rangle = n^i_{Co} b_{Co} + n^i_{Ti} b_{Ti} + (1 - n^i_{Co} - n^i_{Ti}) b_{Fe} \quad [1]$$
$$i = 2a, 4e, 12k, 4fVI, 4fIV,$$

where n^i represents the occupation factor at the i-site of Co and Ti ions. The total amount of doping cations that have entered the structure per formula unit will be

$$x_c = \sum_i m^i n^i_{Co} = \sum_i m^i n^i_{Ti}, \quad [2]$$

where m^i represents the crystallographic multiplicity of the i-site divided by the number of formula unit per unit cell.

Thus, from the experimental values for $\langle b^i \rangle$ and using the five equations [1] and [2], the cationic distribution (n^i_{Co} and n^i_{Ti}) can, in principle, be calculated.

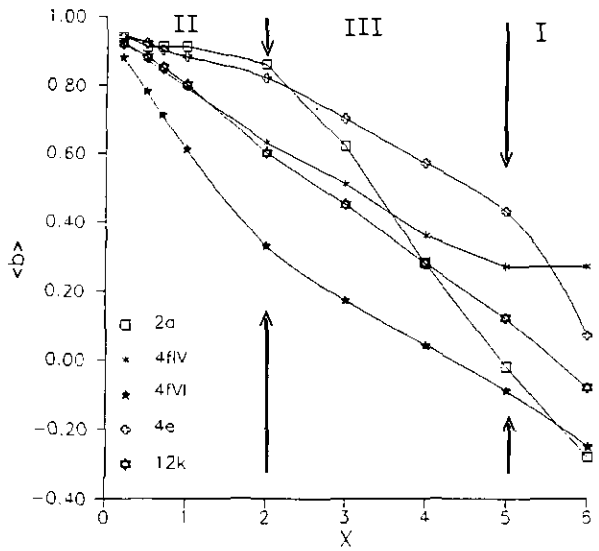

FIG. 4. Refined average scattering lengths $\langle b \rangle$ corresponding to the five metallic sublattices as a function of the doping rate x. All the represented values are given in 10^{-12} cm. (The values corresponding to $0.2 \leq x \leq 1$ are taken from Ref. (10)).

Figure 4 shows the refined average scattering lengths, $\langle b^i \rangle$, corresponding to the five metallic sublattices as a function of the doping rate x. The overall decrease of $\langle b^i \rangle$ is indicative of the presence of Co and/or Ti in all sublattices. However, the evolution of $\langle b^i \rangle$ is not the same in the five metallic positions nor in all the composition range. Looking at Fig. 4 and in order to determine the cationic distribution, the $BaFe_{12-2x}Co_xTi_xO_{19}$ system could be divided into three regions:

I. $x = 6$;

II. $0 < x \leq 2$;

III. $2 \leq x \leq 5$.

I. $x = 6$ *(*$BaCo_6Ti_6O_{19}$*).* In this composition, Fe^{3+} ions have been totally substituted for by Co^{2+} and Ti^{4+}. The solution of Eq. [1] gives the cation distribution directly for each position without it being necessary to introduce any hypothesis. The results obtained (Table 2) indicate that practically all sublattices are occupied by both cations. One exception is the tetrahedral $4f$IV site, where only Co(II) ions are located.

Thus, the Ti^{4+} ions do not enter tetrahedral sites (only 3% of the total amount of Ti^{4+} is located in the $4e$ sublattice) and they prefer $2a$ and $4f$VI octahedral positions. Moreover, the Co^{2+} ions clearly prefer the tetrahedral sites ($4e$ and $4f$IV). Only a small amount of Co^{2+} ions enter the $2a$ and $4f$VI sublattices.

Thus, the hierarchy of preferences as a function of n^i values is:

$$\text{Ti(IV)}: 2a \approx 4f\text{VI} > 12k > 4e$$

$$\text{Co(II)}: 4f\text{IV} > 4e > 12k > 2a \approx 4f\text{VI}.$$

II. $0 < x \leq 2$. In this region, the average scattering length of the $2a$ and $4e$ positions is nearly constant, indi-

TABLE 2
Occupation Factor (fraction), n^i, for Fe(III), Co(II), and Ti(IV) Ions in Each Sublattice as a Function of x

Nominal composition x	Atom	Sublattice					Calculated composition x_c
		$2a$	$4f$IV	$4f$VI	$4e(1/2)$	$12k$	
1[a]	Fe(III)	.96	.76	.73	.90	.84	
	Co(II)	—	.24	—	.10	.08	
	Ti(IV)	.04	—	.27	—	.08	1.0
2	Fe(III)	.92(1)	.54(1)	.52(1)	.82(1)	.65(2)	
	Co(II)	—	.46(1)	—	.18(1)	.17(1)	
	Ti(IV)	.08(1)	—	.48(1)	—	.18(1)	2.1(1)
3	Fe(III)	.73(1)	.38(1)	.36(7)	.65(1)	.51(4)	
	Co(II)	—	.62(1)	.07(5)	.35(1)	.22(1)	
	Ti(IV)	.27(1)	—	.57(1)	—	.27(1)	3.0(2)
4	Fe(III)	.48(1)	.16(1)	.24(7)	.46(1)	.35(4)	
	Co(II)	—	.84(1)	.10(5)	.54(1)	.28(2)	
	Ti(IV)	.52(1)	—	.66(2)	—	.37(1)	4.1(1)
5	Fe(III)	.24(1)	—	.13(7)	.25(1)	.20(4)	
	Co(II)	—	1.00(4)	—	.75(1)	.34(2)	
	Ti(IV)	.76(1)	—	.75(2)	—	.46(2)	5.0(2)
6	Co(II)	.17(2)	1.00(4)	.17(2)	.80(2)	.450(5)	
	Ti(IV)	.83(2)	—	.83(2)	.20(2)	.550(5)	6.0(1)

[a] n_{Fe}, n_{Co}, and n_{Ti} values taken from Ref. (10).

cating that most of such sites will be occupied by Fe(III) ions. For $4fIV$, $12k$, and $4fVI$, the $\langle b^i \rangle$ values decrease as x increases (Fig. 4). Batlle *et al.* (10, 16) studied the composition range $0.2 \leq x \leq 1$ and they established some constraining hypotheses in order to determine the cation distribution. Up to $x = 2$, the evolution of the average scattering lengths seems to be continuous for all the five metallic sublattices (see Fig. 4). This fact suggests that we can still use the same hypothesis as in (10) for this compositional range.

According to the results obtained for $x = 6$, these hypotheses can be accepted: the Ti^{4+} ions do not enter tetrahedral sublattices and no Co^{2+} ions go to the $2a$ positions. Then, Eq. [1] allows us to unambiguously derive the cationic distribution for the $4fIV$, $4e$, and $2a$ metallic sublattices.

Concerning the occupation factor n_{Co}, n_{Ti} in the $4fVI$ and $12k$ positions, Batlle *et al.* (10) restrict all the possible occupancies between two limiting cases. They parametrize these two limiting cases by means of the ratio of occupation parameters of the Co ions in the $12k$ and $4fVI$ sublattices:

	n^{12k}/n^{4fVI} (Co)	n^{12k}/n^{4fVI} (Ti)
A limit	∞	~0.26
B limit	0	~1.33.

According to the present results obtained for Ba $Co_6Ti_6O_{19}$, the B limit, in which no Co^{2+} ions are located in the $12k$ sublattice, should be excluded. In this sense, the hierarchy of preferences is

Fe(III): $2a > 4e > 12k > 4fIV > 4fVI$

Ti(IV): $4fVI > 12k > 2a$

Co(II): $4fIV > 4e > 12k$.

III. $2 \leq x \leq 5$. For this composition range, the Co(II) and Ti(IV) amount introduced into the structure is considerable (>50%). This fact is reflected in a pronounced decrease in $\langle b \rangle$ for the $2a$ site (Fig. 4), which could be due to a more pronounced entering of Ti^{4+} ions into this sublattice (the scattering length of Ti is negative). Moreover, a change in the slope for the $4fVI$ site, which remains constant until $x = 6$, is also observed. This variation could be associated with the introduction of Co(II) ions in this position, only occupied by Fe^{3+} and Ti^{4+} for $x \leq 2$.

For the other sublattices ($4fIV$, $4e$, and $12k$), the average scattering length linearly decreases to $x = 5$.

Then, according to the results obtained for $x = 6$, the hypotheses assumed in Region II can still be maintained (the Ti ions are not located in tetrahedral sites, and Co ions are not introduced into the $2a$ site). Thus, the cationic distribution in this composition range could be

$2a$: Fe(III), Ti(IV)

$12k$, $4fVI$: Fe(III), Ti(IV), Co(II)

$4e$, $4fIV$: Fe(III), Co(II).

The solution of Eq. [1] gives the cationic distribution directly for the $2a$, $4fIV$, and $4e$ metallic sublattices. It is not the case for $4fVI$ and $12k$ positions, where three cations are introduced. The parametrization adopted for the cationic distribution in Region II produces many different solutions. Thus, the available data are not sufficient to unambiguously determine the cation distribution. We have looked for other alternatives to get a consistent cation distribution. Considering the tendency of Ti(IV) ions to be located in the $4fVI$ sublattice, a linear law for n_{Ti} in this position can be assumed from $x = 2$ to $x = 6$. With this alternative hypothesis, the population parameters, n_{Co}, n_{Ti}, for each sublattice can be obtained (Table 2). According to that, the following hierarchy of preferences could be proposed:

Fe(III): $2a \approx 4e > 12k \geq 4fVI > 4fIV$

Ti(IV): $4fVI > 2a > 12k$

Co(II): $4fIV > 4e > 12k > 4fVI$.

TABLE 3
Structural Parameters from Neutron Powder Diffraction at 298 K

	Position	x	y	z	B (Å^2)
		$BaFe_4Co_4Ti_4O_{19}$			
Ba	$2d$	2/3	1/3	0.25	0.40(11)
Me1	$2a$	0	0	0	0.25(7)
Me2	$4f$(IV)	1/3	2/3	0.0250(4)	0.25(7)
Me3	$4f$(VI)	1/3	2/3	0.189(2)	0.25(7)
Me4	$4e$(1/2)	0	0	0.2607(3)	0.25(7)
Me5	$12k$	0.167(1)	$2x$	−0.1058(2)	0.25(7)
O1	$4e$	0.0000	0.0000	0.1512(2)	0.94(2)
O2	$4f$	1/3	2/3	−0.0581(3)	0.94(2)
O3	$6h$	0.1870(9)	$2x$	0.25	0.94(2)
O4	$12k$	0.1517(5)	$2x$	0.0529(1)	0.94(2)
O5	$12k$	0.500(1)	$2x$	0.1507(1)	0.94(2)
	$R_{wp} = 7.08$, $R_B = 5.48$, $R_{exp} = 4.78$, $\chi^2 = 2.20$				
		$BaCo_6Ti_6O_{19}$			
Ba	$2d$	2/3	1/3	0.25	0.50(12)
Me1	$2a$	0	0	0	0.53(8)
Me2	$4f$(IV)	1/3	2/3	0.0251(5)	0.53(8)
Me3	$4f$(VI)	1/3	2/3	0.1912(5)	0.53(8)
Me4	$4e$(1/2)	0	0	0.2540(23)	0.53(8)
Me5	$12k$	0.173(4)	$2x$	−0.1082(6)	0.53(8)
O1	$4e$	0	0	0.1508(2)	0.96(2)
O2	$4f$	1/3	2/3	−0.0581(2)	0.96(2)
O3	$6h$	0.1873(8)	$2x$	0.25	0.96(2)
O4	$12k$	0.1498(5)	$2x$	0.0524(1)	0.96(2)
O5	$12k$	0.5000(8)	$2x$	0.1506(1)	0.96(2)
	$R_{wp} = 6.96$, $R_B = 6.01$, $R_{exp} = 4.82$, $\chi^2 = 2.09$				

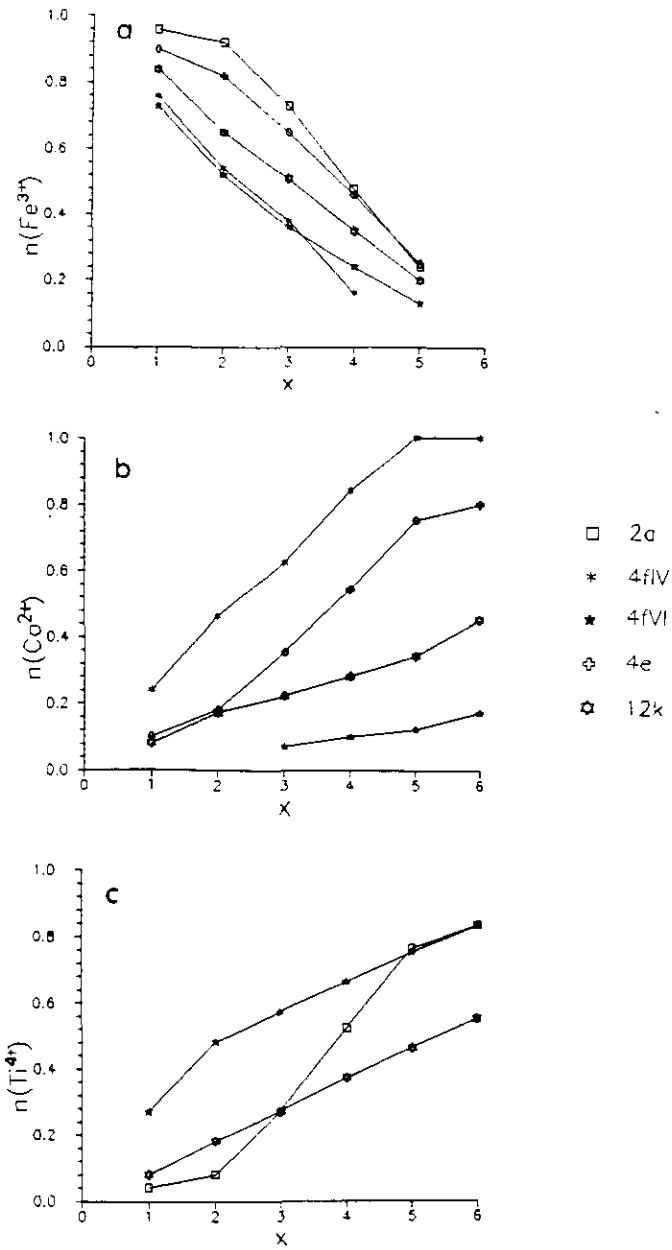

FIG. 5. Fraction of (a) Fe^{3+}, (b) Co^{2+}, and (c) Ti^{4+} in each sublattice as a function of x.

The final results for the cationic distribution of each sublattice in the whole compositional range ($1 \leq x \leq 6$) are given in Table 2. A good agreement between the nominal (x) and the calculated composition from Eq. [2] (x_c) is observed. In Fig. 5, the occupation of Fe, Ti, and Co ions in all sublattices is displayed.

From a crystallographic point of view, we have compared the coordination polyhedra of the extreme members of the solid solution: $BaFe_{12}O_{19}$ (data taken from Ref. (5)) and $BaCo_6Ti_6O_{19}$ and the intermediate composition $BaFe_4Co_4Ti_4O_{19}$. Table 3 shows the atomic positions obtained from structure refinements at 298 K for $x = 4$ and $x = 6$.

The interatomic distances calculated from these atomic positions with their standard deviations are given in Table 4.

DISCUSSION

The above results show the preferential substitution of Ti^{4+} ions in octahedral positions and fundamentally in $4fVI$ sublattices (face-shared octahedral). This solution is equivalent to that observed in $BaTiO_3$ (17) or R-$BaTi_2Fe_4O_{11}$ (18). However, the electrostatic repulsions present in this position could be due, for $x > 2$, to a bigger amount of Ti ions beginning to occupy the $2a$ site. For $x = 6$, 3% Ti ions are located in $4e$ positions. Although this position is not very common in the Ti(IV) ions, we can find it in a fivefold coordination position in the $KTiO_{2.5}$ compound (19). On the other hand, the Co(II) ions show a high tendency for the tetrahedral metallic sublattices, fundamentally for $4fIV$ position. This marked preference for the tetrahedral sites is also observed in other ferrites, $Ba_2Co_2Fe_{11}O_{22}$ (20) and $BaCo_2Fe_{16}O_{27}$ (21). For $x = 5$, the $4fIV$ sublattice is saturated and no more Co ions can go there. Then, for $x = 6$, a small amount of Co ions must enter into the $2a$ octahedral site. At this point, it is worth mentioning that neutron diffraction is the most powerful tool to determine the cationic distribution, since a large number of cationic distributions among the metallic sublattices of these hexagonal structures is possible. In fact, previous studies on the location of Co^{2+} ions from both saturation magnetization and microwave ferromagnetic resonance measurements (22, 23) suggested a preference of Co^{2+} ions for octahedral rather than tetrahedral sites.

In the same way, the fact that Co(II) ions fundamentally occupy the tetrahedral sites and Ti(IV) ions the octahedral positions could justify the facility of formation of the solid solution in all the composition range.

However, the ion preference for a given position depends on both the ion characteristics and the nature of the other ions present in the compound. For instance, in the $BaFe_{12-2x}Mg_xTi_xO_{19}$ system ($0 \leq x \leq 6$) studied by Kalvoda *et al.* (24), the Ti^{4+} ions are located, mainly, in $2a$ and $4e$ positions for $x = 6$ (when M(II) = Co, only a small amount of Ti ions is introduced in the $4e$ sublattice). Besides, in the $BaFe_{12-2x}Co_xSn_xO_{19}$ system ($0 \leq x \leq 1$) (25), Co(II) has a marked preference for $4fIV$ and $4fVI$ positions ($x \leq 0.6$). However, when M(IV) = Ti, the Co^{2+} ions only occupy the $4fVI$ position for $x \geq 2$. This different tendency of Co^{2+} ions to enter each sublattice when M(IV) = Ti or Sn seems to be the reason for the different properties shown by both systems (26).

From these results, it can be concluded that three regions exist in the $0.2 \leq x \leq 6$ composition range of the

$BaFe_{12-2x}Co_xTi_xO_{19}$ system, since the tendency of Co(II) and Ti(IV) ions for going into the five sublattices is different (27). The hierarchy of preferences of these ions is modified as the Co–Ti content increases because of the perturbed charge distribution among the different sublattices.

From a magnetic point of view, the cationic substitution originates a complicated sequence of magnetic structures that is difficult to analyze with a powder sample. In this sense, the total substitution of Fe^{3+} by Co^{2+} and Ti^{4+} leads to a highly diluted magnetic material, $BaCo_6Ti_6O_{19}$, showing a strong magnetic frustration, which presents a spin–glass transition at $T_f = 13.6$ K (28, 29).

From Table 4, we can observe that some interatomic distances of the members $x = 4$ and $x = 6$ increase and others decrease with respect to the parent $BaFe_{12}O_{19}$ (5). We shall try to explain the overall features of the distance variations from the observed cationic distribution.

It is worth mentioning that the cation–cation distance in the 4*f*VI sublattice, constituting face-shared octahedra, increases (see Table 4) from $x = 0$ to $x = 4$, but decreases at $x = 6$. This effect is also observed in the $SrFe_{12-x}Al_xO_{19}$ system (30), in which Al(III) ions are located in this position. This could be due to a dominant effect of the repulsive forces between Ti^{4+}, a critical Ti^{4+} content being reached, from which the smaller ionic radius favors a shorter distance between both cations.

In the same way, the cation deviation from the BaO_3 mirror plane in the 4*e*(1/2) position (1/2 *d*(Me4–Me4) in Table 4) increases from $x = 0$ (0.17 Å) to $x = 4$ (0.25 Å) and afterwards decreases for $x = 6$ (0.09 Å). This behavior could be related to a tendency of Co^{2+} for going to tetrahedral positions, thus increasing the effective amplitude of the local diffusion between the two pseudotetrahedral 4*e* positions. The decrease of the amplitude for $x = 6$ could be due to the introduction of Ti^{4+}, which seems to be, locally, well fixed in the position 2*b* on the mirror plane.

The obtained average distances, $d\langle$Me–O$\rangle$, seem to be in good agreement with the cationic distribution. An increase of $d\langle$Me–O$\rangle$ for a given sublattice is observed when the "average ionic radius" of the effective ion occupying it increases, and vice versa. The average $d\langle$Me–O$\rangle$ for the tetrahedral sublattices (4*f*IV and 4*e*), occupied mainly by Co^{2+} ions, increases due to a higher radius of Co(II) (31) ($^{IV}r_{Co^{2+}} = 0.58$ Å, $^{IV}r_{Fe^{3+}} = 0.49$ Å). The increase is larger going from $x = 0$ to $x = 4$, while for $x = 6$, a lower increase is observed due to a smaller occupation of Co^{2+} ions. The opposite effect holds in the 2*a* sublattice, where Ti^{4+} ions with a lower ionic radius ($^{VI}r_{Ti^{4+}} = 0.605$ Å; $^{VI}r_{Fe^{3+}} = 0.645$ Å) are located. On the other hand, the presence of Fe(III), Ti(IV), and Co(II) ions in the 12*k* and 4*f*VI octahedral positions, with different ionic radius ($^{VI}r_{Co^{2+}} = 0.745$ Å), compensates the volume variation.

It is worth testing the cationic distribution against the observed average Me–O distances in a more quantitative way. In fact, all the above qualitative considerations can be put in a quantitative basis, using the unifying method of valence bonds as formulated in Refs. (32, 33). This method allows us to "predict" the average distance expected for a site occupied by an "average chemical species."

For a single chemical species of valence V located in a coordination polyhedron of N corners, the distance is

TABLE 4
Important Distances in the $BaFe_{12}O_{19}$, $BaFe_4Co_4Ti_4O_{19}$, and $BaCo_6Ti_6O_{19}$ Compounds

		$x = 0^a$	$x = 4$	$x = 6$
		Ba (2*d R* block)		
Ba–O3	×6	2.950(2)	2.960(6)	2.966(4)
Ba–O5	×6	2.868(2)	2.877(3)	2.884(3)
⟨Ba–O⟩		2.909	2.918	2.925
		Me1 (2*a S* block)		
Me1–O4	×6	2.000(2)	1.983(2)	1.964(2)
⟨Me1–O⟩		2.000	1.983	1.964
		Me2 (4*f*IV *S* block)		
Me2–O2	×1	1.894(3)	1.94(1)	1.94(1)
Me2–O4	×3	1.894(2)	1.967(4)	1.986(4)
⟨Me2–O⟩		1.894	1.967)	1.986
		Me3 (4*f*VI *R* block)		
Me3–O3	×3	2.073(2)	2.07(3)	2.032(8)
Me3–O5	×3	1.969(2)	1.92(2)	1.953(6)
⟨Me3–O⟩		2.021	1.99	1.992
Me3–Me3		2.768(1)	2.85(6)	2.75(1)
		Me4 (4*e*(1/2)–2*b R* block)		
Me4–O1	×1	2.128(3) (2.298(3))^b	2.056(8) (2.306(5))^b	2.22(2) (2.318(5))^b
Me4–O1	×1	2.468(3) (2.298(3))^b	2.556(8) (2.306(5))^b	2.41(2) (2.318(5))^b
Me4–O3	×3	1.867(2) (1.859(2))^b	1.929(6) (1.913(4))^b	1.922(4) (1.919(5))^b
⟨Me4–O⟩		2.039 (2.035)^b	2.080 (2.070)^b	2.08 (2.079)^b
Me4–Me4		0.340(1)	0.499(9)	0.19(7)
		Me5 (12*k R–S* interphase)		
Me5–O1	×1	1.985(2)	2.010(5)	2.03(2)
Me5–O2	×1	2.095(4)	2.033(6)	2.02(2)
Me5–O4	×2	2.114(3)	2.049(6)	2.12(2)
Me5–O5	×2	1.932(3)	1.998(8)	1.95(2)
⟨Me5–O⟩		2.028	2.023	2.03

Note. The large standard deviation observed for some Me–O distances corresponds to sites where the average chemical species occupying it give a very low effective scattering length.

[a] Data for $x = 0$ taked from Obradors *et al.* (5).

[b] Distances with the Me atom occupying the bipyramidal cavity, centered in Wyckoff position 2*b*.

TABLE 5
Predicted Distances ($\bar{d}_i$) (Eq. [3]) for Each Cation in Different Coordination Polyhedra

$\bar{d}_i$	$N = 4$	$N = 5$	$N = 6$
Fe(III)	1.865	1.948	2.015
Co(II)	1.815	1.897	1.965
Ti(IV)	1.948	2.031	2.098

Note. $B = 0.37$ Å; $R_0Co^{2+} = 1.692(5)$ Å; $R_0Fe^{3+} = 1.759(3)$ Å; $R_0Ti^{4+} = 1.85(4)$ Å.

TABLE 6
Expected Distances According to Eq. [4] ($\langle d_{expt} \rangle$) and Observed Averaged Distances ($\langle d_{obs} \rangle$) for Each Sublattice

	$x = 0$		$x = 4$		$x = 6$	
Sublattice	$\langle d_{obs} \rangle$	$\langle d_{expt} \rangle$	$\langle d_{obs} \rangle$	$\langle d_{expt} \rangle$	$\langle d_{obs} \rangle$	$\langle d_{expt} \rangle$
Me1 (2*a*)	2.000	2.015	1.983	1.989	1.964	1.987
Me2 (4*f*IV)	1.894	1.865	1.967	1.935	1.986	1.948
Me3 (4*f*VI)	2.021	2.015	1.99	1.990	1.992	1.987
Me4 (4*e*–2*b*)	2.039 (2.035)[a]	1.948	2.080 (2.070)[a]	1.993	2.08 (2.079)[a]	2.004
Me5 (12*k*)	2.028	2.015	2.023	2.020	2.03	2.025

[a] Observed average distance with the Me atom centered in position 2*b*.

given by the expression

$$\bar{d} = R_0 - B \ln(V/N), \quad [3]$$

where R_0 and B are characteristic of the particular cation–anion pair (32).

If a site is occupied by several chemical species, the expected average distance is given by

$$\langle d_{expt} \rangle = \Sigma\, n_i \bar{d}_i, \quad [4]$$

where n_i is the fraction of the chemical species for which the predicted distance for the site is $\bar{d}_i$. The numbers n_i are collected in Table 2 and the "predicted" distances $\bar{d}_i$ are given in Table 5.

The expected distances given by Eq. [4] are collected together with the observed average distance for each sublattice in Table 6. As can be seen, except for the bipyramidal site, which violates the valence bond sums even in the parent $x = 0$ compound, the comparison of the two sets of distances shows that the absolute value of their difference is below 0.04 Å (for the 4*e*(1/2)–2*b* position, the difference is about 0.08 Å). We have to keep in mind that the extent to which the valence bond sum rule is satisfied in compounds with several atoms in special positions is about 3 to 5% in predicted distances. For that reason, the cationic distribution cannot be determined solely from the observed average distances. What we have shown with the results of Table 6, is that the proposed cation distribution is perfectly compatible with the observed average Me–O distances.

CONCLUSIONS

We have determined the cationic distribution in a complex system in which the presence of three different chemical species, which can occupy the same crystallographic position, makes the diffraction data ambiguous. The use of additional hypotheses is necessary to achieve a unique solution. These hypotheses are fully supported by the consistency of all the crystal chemistry parameters available from the structure refinements.

ACKNOWLEDGMENTS

The authors are grateful to Drs. X. Batlle and X. Obradors for helpful discussions. Financial support from the Comision Interministerial de Ciencia y Tecnología (CICYT, Spain) through projects MAT91-0331 and MAT93-0207 is also acknowledged.

REFERENCES

1. J. Smith and H. P. J. Wijn, "Ferrites." Philips Technical Library, Eindhoven, 1960.
2. H. Kojima, *in* "Ferromagnetic Materials" (E. P. Wohlfarth, Ed.), Vol. 3, p. 305. North-Holland, Amsterdam, 1982.
3. O. Kubo, T. Ido, H. Yokoyama, and Y. Koike, *J. Appl. Phys.* **57,** 4280 (1985).
4. W. D. Townes, J. H. Fang, and A. S. Perrotta, *Z. Kristallogr.* **125,** 437 (1967).
5. X. Obradors, A. Collomb, M. Pernet, D. Samaras, and J. C. Joubert, *J. Solid State Chem.* **56,** 171 (1985). See also J. Fontcuberta, W. Reiff, and X. Obradors, *J. Phys.: Condens. Matter* **3,** 2131 (1991).
6. E. W. Gorter, *Proc. IEEE* **104,** 225 (1957).
7. G. Albanese, *J. Phys.* **38,** C1-85 (1977).
8. G. Albanese, A. Deriv, E. Lucchini, and G. Slokar, *Appl. Phys. A* **26,** 45 (1981).
9. A. Sadykov, O. P. Aleskko-Ozhevskii, and N. A. Arten'em, *Sov. Phys. Solid State* **23,** 1090 (1981).
10. X. Batlle, X. Obradors, J. Rodríguez-Carvajal, M. Pernet, M. V. Cabañas, and M. Vallet-Regí, *J. Appl. Phys.* **70,** 1614 (1991).
11. Y. K. Hong, Y. J. Paig, D. G. Agresti, and T. D. Shelfer, *J. Appl. Phys.* **61,** 3872 (1987).
12. F. Chou, X. Feng, J. Liu, and Y. Liu, *J. Appl. Phys.* **61,** 3881 (1987).
13. H. Stepankova, J. Kohout, and Z. Simsa, *J. Magn. Magn. Mater.* **104–107,** 411 (1992).
14. L. Vegard, *Z. Phys.* **5,** 393 (1921).
15. J. Rodríguez, M. Anne, and J. Pannetier, "STRAP," Institut Laue-Langevin Internal Report 87Ro14T, 1987.
16. X. Batlle, X. Obradors, M. Pernet, M. Vallet-Regí, M. V. Cabañas, J. Rodríguez, and J. Fontcuberta, *J. Magn. Magn. Mater.* **83,** 465 (1990).
17. R. D. Burbank and H. T. Evans, *Acta Cryst.* **1,** 330 (1948).
18. M. C. Cadée and D. J. W. Ijdo, *J. Solid State Chem.* **53,** 302 (1984).
19. S. Anderson and A. D. Wadsley, *Acta Chem. Scand.* **15,** 663 (1961).
20. A. Collomb, M. A. HadjFarhat, and J. C. Joubert, *Mater. Res. Bull.* **24,** 459 (1989).

21. A. Collomb, P. Wolfers, and X. Obradors, *J. Magn. Magn. Mater.* **62,** 57 (1986).
22. J. Smit, F. K. Lotgering, and E. U. Enz, *J. Appl. Phys.* **31,** 137 (1960).
23. D. J. De Bitetto, *J. Appl. Phys.* **35,** 3482 (1964).
24. L. Kalvoda, M. Dlovhá, S. Vratislav, and J. Jirak, *J. Magn. Magn. Mater.* **87,** 243 (1990).
25. X. Batlle, J. Rodríguez, X. Obradors, M. Pernet, M. Vallet, and J. Fontcuberta, *J. Phys.* **49,** C8-939 (1988).
26. X. Batlle, M. Pernet, X. Obradors, and M. Vallet-Regí *in* "Advances in Ferrites" (C. M. Srivastava and M. J. Patni, Eds.), p. 423. Oxford and IBH, New Delhi, 1989.
27. X. Batlle, M. V. Cabañas, X. Obradors, M. Vallet, and J. Rodríguez *in* "Spanish Contribution to Neutron Scattering Techniques" (J. C. Gomez-Sal *et al.*, Eds.), p. 47. 1991.
28. X. Batlle, A. Labarta, X. Obradors, M. V. Cabañas, and M. Vallet-Regí, *J. Appl. Phys.* **70,** 6172 (1991).
29. A. Labarta, X. Batlle, B. Martínez, and X. Obradors, *Phys. Rev.* **46,** 8994 (1992).
30. F. Sandiumenge, S. Gali, and J. Rodríguez, *Mater. Res. Bull.* **23,** 685 (1988).
31. R. D. Shannon, *Acta Crystallogr. Sect. A* **32,** 751 (1976).
32. I. D. Brown and D. Altermatt, *Acta Crystallogr. Sect. B* **41,** 244 (1985).
33. I. D. Brown, *Acta Crystallogr. Sect. B* **48,** 553 (1992).